Determination of Sr isotopes in calcium phosphates using laser ablation inductively coupled plasma mass spectrometry and their application to archaeological tooth enamel

M.S.A. Horstwood[1*], J.A. Evans[1] & J. Montgomery[2]

[1] NERC Isotope Geosciences Laboratory, British Geological Survey, UK

[2] Division of Archaeological, Geographical and Environmental Sciences, School of Life Sciences, University of Bradford, UK

* Corresponding author – msah@nigl.nerc.ac.uk

1. ABSTRACT

The determination of accurate Sr isotope ratios in calcium phosphate matrices by laser ablation multi-collector ICP-MS is demonstrated as possible even with low Sr concentration archaeological material. Multiple on-line interference correction routines for doubly-charged REE, Ca dimers and Rb with additional calibration against TIMS-characterised materials are required to achieve this. The calibration strategy proposed uses both inorganic and biogenic apatite matrices to monitor and correct for a ^{40}Ca-^{31}P-^{16}O polyatomic present at levels of 0.3-1% of the non-oxide peak, which interferes on ^{87}Sr causing inaccuracies of 0.03-0.4% in the $^{87}Sr/^{86}Sr$ isotope ratio. The possibility also exists for synthetic materials to be used in this calibration. After correction for interferences total combined uncertainties of 0.04-0.15% (2SD) are achieved for analyses of 13-24ug of archaeological tooth enamel with Sr concentrations of *c.*100-500ppm using MC-ICP-MS. In particular, for samples containing >300ppm Sr, total uncertainties of ~0.05% are possible utilising 7-12ng Sr. Data quality is monitored by determination of $^{84}Sr/^{86}Sr$ ratios.

When applied to an archaeological cattle tooth this approach shows Sr-isotope variations along the length of the tooth in agreement with independent TIMS data. The ^{40}Ca-^{31}P-^{16}O polyatomic interference is the root cause of the bias at mass 87 during laser ablation ICP-MS analysis of inorganic and biogenic calcium phosphate (apatite) matrices. This results in inaccurate $^{87}Sr/^{86}Sr$ ratios even after correction of Ca dimers and doubly charged rare earth elements. This interference is essentially constant at specific ablation conditions and therefore the effect on $^{87}Sr/^{86}Sr$ data varies in proportion to changes in the Sr concentration of the ablated material. Complete elimination of this interference is unlikely through normal analytical mechanisms and

therefore represents a limitation on the achievable accuracy of LA-(MC-)ICP-MS $^{87}Sr/^{86}Sr$ data without rigorous calibration to known reference materials.

Keywords: laser ablation, ICP-MS, Sr isotopes, phosphate, apatite, archaeology, tooth, enamel

2. INTRODUCTION

Strontium isotope analysis has traditionally used thermal ionisation mass spectrometry (TIMS) to discriminate between natural materials of different origin. The most recent of these studies has used TIMS analyses of *c.*4μg micro-milled samples (~3-10ng Sr) to demonstrate Sr isotope variations in magmatic crystals sampled in thick section (Charlier et al. (2006)). The advent of multi-collector inductively coupled plasma mass spectrometry (MC-ICP-MS), coupled with laser ablation (LA) sample introduction, provides the possibility to measure Sr isotope variations at higher spatial resolutions (*c.*50-100μm), with faster analysis times and less damage to the samples than is generally achieved with traditional TIMS methodologies.

Studies to date have demonstrated, to varying degrees, the ability of LA-ICP-MS techniques to measure Sr isotope variations in carbonate (Woodhead et al.(2005)), feldspar (Davidson et al.(2001)) and other materials (Waight et al. (2002), Schmidtberger et al.(2003), Ramos et al (2004),). However, despite an initial paper by Prohaska et al. (2002) documenting $^{87}Sr/^{86}Sr$ analysis of human bone using LA-quadrupole-ICP-MS and a paper by Bizzarro et al. (2003) who used high-Sr apatites, laser ablation analysis of phosphate materials has not figured prominently in the scientific literature. The reason for this lies in the considerable analytical difficulties involved in generating accurate $^{87}Sr/^{86}Sr$ ratios for samples with Sr concentrations in the 100's ppm range (e.g. Richards et al (2007)). These difficulties include known isobaric interferences (^{87}Rb), doubly-charged REE ions (Paton et al (2007)) and polyatomic species such as Ca dimers (Woodhead et al (2005)) and other molecular species (Horstwood and Evans (2002), Horstwood and Nowell (2005), Simonetti et al. (2007), Simonetti et al. (2008)).

The $^{87}Sr/^{86}Sr$ isotope variation in tooth enamel is of particular interest to archaeological studies of human and animal migration as enamel is highly resistant to diagenetic processes and preserves isotopic and elemental 'life signals' in both fossil and archaeological teeth (Bocherens et al. (1994); Horn et al. (1994); Wang and Cerling (1994); Rink and Schwarcz (1995); Michel et al. (1996); Koch et al. (1997); Budd et al. (2000); Hoppe et al. (2003); Trickett et al. (2003); Dauphin and Williams (2004); Montgomery et al. (2007)). This allows the use of strontium as a tracer of human and animal migration in the past (see Beard and Johnson (2000); Bentley (2006) and references therein). Analysis of Sr isotope compositions of enamel has traditionally required thermal ionisation mass spectrometry (TIMS). The sampling technique for these relatively low concentration materials (*c.*50-300ppm Sr) has historically required the slicing or drilling of 10-50mg of tooth enamel to obtain enough dentine-free enamel for analysis. Such destructive sampling commonly raises concerns when analysing precious and rare material. A technique that leaves the specimen essentially intact, with as little damage as possible, would therefore be a great advantage. LA-ICP-MS provides just such a technique.

In this paper we demonstrate the presence of a Ca-P-O polyatomic interference during LA-ICP-MS analysis of phosphate matrices, in addition to previously recognised interferences, and describe a method for its correction. We illustrate the effectiveness of the correction routines and their significance for archaeological studies by application to a cattle tooth associated with an Iron Age chariot burial.

3. ANALYTICAL METHODOLOGY

3.1 Description of samples and sample preparation.

Nine tooth enamel samples, two igneous apatites and a modern mollusc shell with Sr isotope compositions previously determined by TIMS (Table 1), were used to define a calibration using LA-MC-ICP-MS. The enamel samples have Sr concentrations ranging from 75-381 ppm, the mollusc shell has a Sr concentration of over 1000 ppm and the highest Sr concentration is in one of the igneous apatites (*c.*35,000 ppm for apatite 326333 of Pearce and Leng (1996)). These high concentration end-members were deliberately chosen to demonstrate the level of accuracy achieved, for phosphate and non-phosphate matrices, by LA-MC-ICP-MS when abundant Sr is available for analysis relative to the interference corrections being applied.

The cattle tooth enamel (representing approximately 1 year of growth) chosen for the case study was selected specifically because it showed a changing composition in Sr concentration and $^{87}Sr/^{86}Sr$ down the tooth crown, on the basis of 2 mm transverse slices by conventional TIMS analysis. A longitudinal section was removed from the entire length of the tooth crown, dentine and cementum were removed, and the enamel sample was bisected longitudinally. One half was sectioned transversely from cusp to cervix to produce 13 *c.*2mm sections that were analysed by TIMS (Table 1). The remaining half was used for the LA study. The possibility for intra-sample heterogeneity is important when comparing conventional TIMS data, derived by the dissolution of *c.*30milligrams of material, with laser ablation analyses sampling 13-24ug. However, little has been written on within-tooth strontium isotope heterogeneity. Montgomery (2002) demonstrated variations of 0.003-0.005% (2σ) for multiple analyses of modern human deciduous and permanent teeth, suggesting minor variations within-tooth and a limiting level of uncertainty for human dental enamel studies. As such, and in light of the fact that TIMS values are used as target values by

which to assess the accuracy of LA-MC-ICP-MS data, all TIMS data are plotted with 0.005% uncertainties.

3.2 Thermal Ionization Mass Spectrometry

Samples were prepared in a class-100 clean chemistry suite by sonicating in high purity water, rinsed twice, dried down in high purity acetone and then placed into pre-cleaned Teflon beakers. An ^{84}Sr tracer was added to the samples before being dissolved in Teflon-distilled 16M HNO_3. Strontium was separated from other components of the sample using conventional Dowex© resin ion-exchange methods. The purified Sr was loaded onto a single Re filament using TaF activator after the method of Birck (1986). $^{87}Sr/^{86}Sr$ isotope compositions and Sr concentrations were determined using a ThermoFinnigan Triton multi-collector mass spectrometer. $^{87}Sr/^{86}Sr$ ratios are normalised to a value of 0.710250 for NBS 987, which averaged 0.710263 ± 0.000008 (2SD, n=50) at the time of analysis using a static acquisition routine.

3.3 LA-MC-ICP-MS

The analytical methodology outlined here used a Nu Plasma HR MC-ICP-MS coupled to a DSN-100 desolvating nebuliser (both from Nu Instruments, UK) and a UP193SS Nd:YAG 193nm laser ablation system (New Wave Research, UK). The mass spectrometer was tuned for maximum sensitivity (~70-100V/ppm, based on solution introduction) and optimised to reduce oxides whilst using 0.8l/min He to flush a standard 30cm^3 laser ablation chamber. All mass spectrometer and laser ablation system set-up parameters are shown in Table EA1. A 213nm laser would equally surfice for this application and hence laser equipments costs are significantly below other alternatives (e.g. femtosecond lasers).

An array of seven Faraday detectors was used with a three-sequence peak jumping routine to allow all the peaks of interest to be acquired. Each sequence acquired 20 ratios of 3 secs integration with a 1 second magnet jump settle time between each. This differs only in overall measurement efficiency when compared to the twelve Faraday, static acquisition procedure documented in Woodhead et al. (2005). Table 2a illustrates the collector configuration used.

During static (or single spot) ablation, particle size distribution and signal intensity decrease as the ablation progresses (Guillong and Günther 2002). A dynamic ablation (or raster) protocol was therefore used in view of the low Sr concentration of the samples, to maintain the signal intensity throughout the analysis. A 425x370µm (X-Y including overlap of spot size) box-raster dynamic ablation pattern and a 100µm ablation spot were used for all phosphate analyses but smaller spot sizes were used for the mollusc shell and inorganic apatite (sample 326333) to reduce the amount of material ablated.

Dynamic ablation produces larger particles (in contrast to static ablation) that ionise less efficiently in the plasma (Guillong and Günther 2002). However, in this instance the benefits of achieving more constant signals for such low concentration samples, outweigh this disadvantage. A single dynamic (raster) analysis ablated down 30-45µm consuming 13-24µg of phosphate, equating to 7-12ng Sr for a sample with a concentration of *c.*500ppm Sr. Although this represents 2-4 times the minimum amount of material required for higher precision microdrill TIMS methodologies on similar concentration materials (see Charlier et al (2006)), laser ablation analysis has its place in terms of saving overall time per sample (in both sample preparation and analysis), the ability to rapidly survey a number of samples for significant variation, the potential to use time-resolved data analysis to resolve variation within the ablated

volume and the overall availability of the technique. It should however be noted that these advantages require a not insignificant investment of energies in processing the data and proving the methodology required (see below).

3.4 Acquisition protocol and interference corrections

All data were acquired using a standard acquisition mode without time-resolved analysis of the signal. A background or on-peak zero (OPZ) was recorded externally for 60secs per sequence prior to every analysis or set of three analyses. In this way interferences from Kr were corrected from the analyses. Woodhead et al (2005) demonstrated this method of Kr correction to be robust and stable. A 30 second instrument baseline, or zero reference point, was recorded during each sample and OPZ analysis by deflecting the voltage on the electro-static analyser.

The $^{87}Rb/^{85}Rb$ ratio for correction of the isobaric interference of ^{87}Rb on ^{87}Sr was determined and/or checked at the start of each analytical session, in the manner described by Nowell et al (2008). Briefly, solutions of Sr reference material NBS 987 were doped with varying levels of Rb, to cover the range of Rb/Sr expected in the samples, and the measured results for $^{87}Total/^{86}Sr$ and $^{85}Rb/^{86}Sr$ regressed (using an $^{86}Sr/^{88}Sr = 0.1194$ for mass bias correction) to find a value for $^{87}Rb/^{85}Rb$, thereby incorporating any differences between the degree of mass bias for the two elements. The determined value was 0.386276 ($R^2 = 0.999999$). This value was then used as the 'true' $^{87}Rb/^{85}Rb$ ratio, inversely corrected for mass bias using the Sr mass bias determined during the ablation, and used to correct the data on-line for Rb interference through measurement of the ^{85}Rb peak. Despite potential differences in mass bias determined via solutions versus during ablation, the size of the corrections described here are small enough as to make any such differences insignificant. For

example, for samples with a Rb/Sr ratio ~0.003, a 10% difference in the mass bias as determined by laser ablation versus that determined by solution and used to inversely correct the 'true' $^{87}Rb/^{85}Rb$ ratio, results in a difference in the $^{87}Sr/^{86}Sr$ ratio of <0.005%.

All ratios required (Table EA2) for the correction of REE and Ca isotope interferences (see Table 2b) were taken from Rosman and Taylor (1998). These ratios were used without inverse correction for mass bias since the mass differences relative to Sr are clearly too large for the Sr mass bias to be appropriate. Equally, the size of the corrections made here are sufficiently small and the combined uncertainty estimate large enough as to make any such differences in the correcting ratios insignificant at present. During ablation, peak intensities at the half-mass positions 81.5 and 83.5 in sequence 1, 85.5 in sequence 2 and 86.5 in sequence 3 were used as monitors of doubly-charged ^{163}Dy, ^{167}Er, ^{171}Yb and ^{173}Yb respectively. These signals were then used to subtract appropriate amounts of relevant doubly-charged on-peak interferences from all Sr peaks using the ratios in Table EA2. To correct for Ca dimers, the remnant signal on the 82 peak, after subtraction of Kr and REE^{2+} ($^{164}Dy^{2+}$ & $^{164}Er^{2+}$) interferences, was assumed to be $^{40}Ca^{42}Ca$ (or $^{40}Ar^{42}Ca$, although the discrimination between species makes little difference due to similar isotopic abundances; see also Woodhead et al (2005)). This peak was then used to determine the amount of, and correct for, $^{40}Ca^{44}Ca$ and $^{40}Ca^{46}Ca$ dimers on peaks 84 and 86 (using the $^{44}Ca/^{42}Ca$ and $^{46}Ca/^{42}Ca$ ratios) in order to correct the stable isotope ratios. Since REE^{2+} and Ca dimer interferences can occur on all masses in the Sr mass range, and the monitor peak for the Ca dimer correction has pre-existing interferences, the order in which the corrections are made is important; this order is REE, then Ca

dimer, then Rb. LA-MC-ICP-MS data are presented in Tables 3a&b and Electronic Annex EA3.

Solution reference material NBS 987 was run before each analytical session with and without Rb doping (Rb/Sr ratios = 0.0003-0.03) to check instrument performance and the veracity of the Rb interference correction. All data are normalised according to the expected $^{84}Sr/^{86}Sr$ and $^{87}Sr/^{86}Sr$ ratios for NBS 987 of 0.0565 and 0.71025 respectively with all uncertainties expressed as relative standard deviations in percent (%). A true $^{86}Sr/^{88}Sr$ ratio of 0.1194 was assumed throughout with all data corrected for instrumental mass bias using an exponential model. All analyses were conducted at a mass resolution ~400, with oxide levels at 0.25-1% quantified through measurement of UO^+/U^+ using a U solution. A desolvated 2% HNO_3 solution was continuously aspirated into the plasma to help maintain plasma conditions and instrumental mass bias between and during different analyses and also provides the necessary Ar make-up gas in the plasma.

4. RESULTS

4.1 Comparison of carbonate and phosphate results and their $^{84}Sr/^{86}Sr$ ratios

A carbonate mollusc shell was analysed in each analytical session to demonstrate the efficacy of the REE^{2+} and Ca dimer corrections. Figure 1a illustrates corrected $^{87}Sr/^{86}Sr$ data acquired on eight analytical sessions over a period of ten weeks. The data average $^{87}Sr/^{86}Sr = 0.709181 \pm 0.0137\%$ (2SD) which is comparable with the uncertainties reported by Woodhead et al (2005; ± 0.0125% (2SD)) for their carbonate laser ablation data. Figure 1b illustrates the $^{84}Sr/^{86}Sr$ ratios for our analyses with and without correction for REE^{2+} and Ca dimer. Total dimer and REE^{2+} corrections constituted 0.83% and 0.0027% of the uncorrected $^{84}Sr/^{86}Sr$ and $^{87}Sr/^{86}Sr$

ratios respectively. These analyses display slightly less dimer formation than the data of Woodhead et al (2005), but also illustrate the importance of correcting for such interferences to achieve more accurate stable isotope ratios to enable monitoring of data quality. The corrected $^{84}Sr/^{86}Sr$ data give an average of 0.0563 ± 0.9% (2SD), slightly below the expected ratio of 0.0565. This may reflect a slight overcorrection of the Ca dimer interference (e.g. due to the presence of $Ar_2H_2^+$) but does not simply reflect use of an incorrect Ca correction ratio since this would require a $^{42}Ca/^{44}Ca$ isotope ratio of *c.*2.3 (instead of *c.*3.2) to achieve an $^{84}Sr/^{86}Sr$ ratio of 0.0565. Inverse mass bias correction of the Ca ratio used for this correction would only lead to lower $^{84}Sr/^{86}Sr$ ratios.

LA-ICP-MS phosphate analyses do not yield accurate $^{87}Sr/^{86}Sr$ ratios even after the application of the REE^{2+}, Ca dimer and Rb corrections. This inaccuracy is correlated with Sr signal during analysis of low Sr concentration phosphates and can be explained if an additional interferent is present, in consistent quantities, on the ^{87}Sr peak. A Ca-P-O polyatomic has been suggested as a likely interferent (Horstwood and Evans (2002), Horstwood and Nowell (2005) and Simonetti et al (2007), Simonetti et al (2008)). Considering the occurrence and significance of a Ca-Ca (or Ar-Ca) dimer molecule during laser ablation analysis of carbonates as demonstrated by Woodhead et al (2005) and corrected for in this protocol, it is reasonable to also consider that a Ca-P dimer molecule is also formed since the $^{31}P^+$ ion should be equally dominant in the plasma during ablation of calcium phosphate matrices. The ubiquitous potential for the generation of oxides in ICP-MS, coupled with the high affinity of phosphorous for oxygen, essentially guarantees the formation of a ^{40}Ca-^{31}P-^{16}O polyatomic molecule which interferes on ^{87}Sr causing high $^{87}Sr/^{86}Sr$ ratios.

The Sr/Ca ratio in biogenic and inorganic apatite is controlled by the strontium concentration as calcium is a stoichiometric component and is therefore essentially constant. Hence, the Ca/Sr (and therefore the Ca-P/Sr, Ca-P-O/Sr and consequently the $^{87}Sr/^{86}Sr$) ratio varies with Sr concentration, between analyses under essentially constant ablation conditions. Therefore, using a set of samples with predetermined compositions, this relationship can be used as a calibration for calcium phosphate samples of unknown Sr isotope composition. We used a set of inorganic and biogenic apatite materials previously characterised by TIMS for this purpose.

After all corrections the average $^{87}Sr/^{86}Sr$ ratio for the Durango apatite is 0.7068 ± 0.03% (2SD). This value is *c.*0.07% higher than the TIMS determined value of 0.706327 (see Table 1). Figures 2a & b show $^{84}Sr/^{86}Sr$ and $^{87}Sr/^{86}Sr$ data respectively for the Durango apatite with and without correction for REE^{2+} and Ca dimer. The total REE^{2+} and Ca dimer contributions to the initial mass bias corrected ratios are more significant than for the carbonate analyses, constituting ~8.4% and ~0.12% of the uncorrected $^{84}Sr/^{86}Sr$ and $^{87}Sr/^{86}Sr$ ratios respectively. After all corrections the average $^{84}Sr/^{86}Sr$ ratio is 0.0564 ± 0.73% (2SD) suggesting all corrections are appropriate. The Durango apatite has significant REE concentrations, the correction for which alone contributes a *c.*6% correction to the uncorrected $^{84}Sr/^{86}Sr$ ratio. The REE^{2+} interference is also the most significant for the $^{87}Sr/^{86}Sr$ ratio with that for the Ca dimer being insignificant. Finally, the Rb correction is insignificant except for two analyses where up to a 0.1% correction of the ratio is required.

Figure 3a (data are presented in Table 3a) illustrates the inaccuracy of the $^{87}Sr/^{86}Sr$ ratio relative to the TIMS determined value for the Durango apatite and tooth calibration materials. This inaccuracy is strongly correlated (R^2 = *c.*0.94) with the

measured Sr signal. Total REE^{2+} and Ca dimer corrections for the tooth calibration materials constitute ~2-11% and ~0.02-0.06% of the uncorrected $^{84}Sr/^{86}Sr$ and $^{87}Sr/^{86}Sr$ ratios respectively. Inaccuracies of up to 10% in the $^{84}Sr/^{86}Sr$ correction will therefore equivalently affect the corrected $^{87}Sr/^{86}Sr$ ratio by only a few 10's ppm. However, equally the $^{84}Sr/^{86}Sr$ ratio is a monitor of the consistency (*c.*0.25-0.5%, 2SD) and accuracy of the OPZ measurement across all the collectors and the $^{86}Sr/^{88}Sr$ mass bias correction (which also has Kr and REE^{2+} interferences on its peaks) and therefore represents an important (and the only) data quality monitor for all these corrections. The relationship of increasing inaccuracy of the $^{87}Sr/^{86}Sr$ ratio with decreasing Sr signal is consistent between different analytical sessions, only varying by the slope of the regression. Taking a high Sr apatite (sample 326333) where REE^{2+} and Ca dimer corrections are insignificant relative to the amount of Sr present, accurate laser ablation $^{87}Sr/^{86}Sr$ ratios can be demonstrated after correction for mass bias (Fig.3b).

Having established the relationship between Sr concentration and interferent level and its potential use in calibrating a set of unknowns, we ran a series of tests to assess the robustness of this calibration and the level of uncertainty at various concentrations and count rates.

4.2 Ca-P-O calibration robustness and Uncertainty Estimation

The correlation between the accuracy of the $^{87}Sr/^{86}Sr$ ratios and the size of the ^{88}Sr peak is shown in Figure 4a for data gathered over 5 of 6 consecutive days. The slope and correlation of these data sets vary each day because of changes in instrument set-up, focus and oxide levels. When the data are normalised to themselves according to their respective regressions, the distribution of points can be used to

assess the uncertainty of the calibration with respect to the different count rates (Figure 4b) using the average and 2SD of triplicate analyses. Three uncertainty ranges can be distinguished with $1/^{88}Sr$ <0.7, 0.7-2, and >2 and uncertainties of 0.042, 0.11 & 0.15% (2SD) respectively. Figure 4c defines a well-correlated regression between the amount of Sr analysed ($1/^{88}Sr$) and the daily uncertainty (2SD, $R^2 = 0.91$, excluding 3 of 25 data points which appear to have fortuitously reproduced too well for the amount of Sr analysed) which can then be used to propagate an appropriate uncertainty for an unknown according to the amount of Sr detected.

4.3 Accuracy of the REE and Ca dimer corrections

We can assess the accuracy of the doubly-charged REE and Ca dimer corrections relative to the average size of the 84 peak, by considering all the $^{84}Sr/^{86}Sr$ data for the apatite and tooth materials acquired over this multi-session period.

Differences between the $^{84}Sr/^{86}Sr$ data before and after the two corrections are shown in Figure 5a. In most cases REE^{2+} contributions to the $^{84}Sr/^{86}Sr$ ratio are small (relative to the dimer correction) but not insignificant, e.g. for the Durango apatite. The Ca dimer correction is quite clearly very significant on the $^{84}Sr/^{86}Sr$ ratio, the significance of which increases with decreasing Sr intensity, the level of dimer formation remaining essentially constant with constant ablation conditions between samples. Looking in detail at the accuracy of both the Ca dimer and REE corrections, Figure 5b illustrates that the data are essentially accurate for all data with more than 10mV total 84. For those data with total 84 signals less than this, which constitutes all the tooth data (both calibration materials and unknowns), there is a clear over-correction of the data resulting in an average $^{84}Sr/^{86}Sr$ of *c.*0.0545, a *c.*3.5% inaccuracy after an initial correction of 14-28% of the original ratio. This inaccuracy

is most likely due to increasingly significant error in the $^{44}Ca/^{42}Ca$ and/or REE ratios used for the corrections, but could also be caused by cumulative inaccuracies in the baseline measurements across the multiple Faraday detectors used for the corrections. Additionally, small interferences as yet unrecognised, may also be affecting baseline and/or on-peak measurements. Taking detection limits as 3SD of the average baseline measurements for a day, Tables 3a&b and Figure 5a demonstrate that even where intensities on the Ca dimer and REE^{2+} interference monitor masses are only marginally above the limit of detection, the corrections for such are warranted. Whatever the cause of the overcorrection, this level of inaccuracy at these levels of signal after such large interference corrections is considered insignificant with regard to the $^{87}Sr/^{86}Sr$ data where the size of the corrections, especially that for Ca dimer, is markedly less relative to the greater ion beam sizes.

4.4 Accuracy of the Ca-P-O calibration correction: a case study

A cattle tooth (mandibular third molar-M3) recovered from a large pit of cattle bones that encircled an Iron Age chariot burial excavated from Magnesian Limestone at Ferry Fryston, UK, was selected as the subject for assessing the accuracy of the Ca-P-O calibration correction. The tooth was sampled in detail and analysed by both TIMS and LA-MC-ICP-MS. A total of 25 laser analyses were made on the tooth over two analytical sessions. Seventeen analyses were made in the principal session where greater spatial resolution was determined. The length of the tooth was measured using a micrometer and used to calibrate the measurements taken from the laser software at the time of analysis. In this way good control on the spatial distribution of the results relative to the TIMS data was achieved for the 425μm x 370μm sample area ablated. The spatial distribution of eight analyses of an earlier session were not controlled in

such detail and a ± 2mm spatial uncertainty has been assigned to these data. These data are presented but focus is placed on the larger data set.

Figure 6a illustrates the Ca-P-O calibration determined at the time of analysis using the Durango apatite and human tooth samples. Figure 6b illustrates the $^{84}Sr/^{86}Sr$ data for the cattle tooth analyses and the data are presented in Table 3b. Initial ratios of *c.*0.062 are corrected to *c.*0.056 after correction for REE^{2+} and Ca dimer interferences. Measurements towards the cusp of the tooth appear to be more overcorrected than towards the cervix despite equivalent 84peak signals (*c.*3.5mV), perhaps reflecting additional unidentified interferences or complicating factors (e.g. organic components within the sample). Again, this level of inaccuracy, considering the large corrections applied to such small signals, is insignificant when compared with the correction protocol applied to the $^{87}Sr/^{86}Sr$ data where the equivalent corrections are much smaller.

Figure 6c plots the $^{87}Sr/^{86}Sr$ data for the Ferry Fryston cattle tooth including the data determined by TIMS. Initial measurements show small but consistent Rb concentrations along the tooth, increasing towards the cusp. After correction for REE^{2+}, Ca dimer and Rb, resultant $^{87}Sr/^{86}Sr$ ratios are still inaccurate relative to TIMS by 0.1-0.2%. However, after calibration to the tooth standards run at the time, agreement between TIMS and laser ablation data is much improved, particularly for the cervical (lower) half of the crown. Figure 6d highlights the total corrected data relative to the TIMS data including the earlier determined smaller laser ablation data set for which spatial control was more limited. Propagating the uncertainties for these data as described, results in total uncertainties on the laser ablation data of 0.1-0.15% (2SD). All data agree, within uncertainty, with the TIMS data.

5. DISCUSSION

5.1 Further analytical considerations

The robustness of the Ca/Sr ratio is demonstrated by the $^{87}Sr/^{86}Sr$ data for the Durango apatite (Figure 2b), which were acquired by varying the ablation conditions (fluence, spot size, etc.) between analyses. Using the TIMS determined $^{87}Sr/^{86}Sr$ ratio to calculate the contribution of the Ca-P-O interference for these Durango apatite analyses, an average interferent level on mass 87 of *c.*6500cps can be shown (Electronic Annex EA3), varying by a factor of two between *c.*4500-9500cps. Ca-P-O contributions for all the other tooth calibration materials analysed during this study can be shown to be of the same order (see Electronic Annex EA3). Oxide levels at the time of analysis were *c.*0.25-1% using UO^+/U^+ as a monitor for the oxide generating potential of the plasma (determined by aspirating a U solution at the time). Although absolute levels of oxide production differ between analytical sessions and between different elemental and ionic species, using U or indeed Ce as a relative proxy to quantify oxide levels is common practice in ICP-MS. For an appropriately tuned plasma typical UO^+/U^+ levels are on the order of ~1% prior to extra reduction measures (e.g. addition of N_2).

A peak of 231,000cps measured during these ablations at mass 71, corresponding to ^{40}Ca-^{31}P, indicates oxide generation for $CaPO^+/CaP^+$ on the order of 2.8% when compared to the calculated 6500cps $^{40}Ca^{31}P^{16}O^+$ interference. A $^{40}Ca^{31}P^{16}O^+$ polyatomic should be accompanied by a very small amount of the $^{44}Ca^{31}P^{16}O^+$ polyatomic at mass 91. Determination of both the $^{40}Ca^{31}P^+$ and $^{44}Ca^{31}P^{16}O^+$ molecular species during analysis of calcium phosphate matrices would allow direct determination and correction of the $^{40}Ca^{31}P^{16}O^+$ interference on ^{87}Sr and

possibly improve data quality. In a separate set of experiments a Nu Instruments AttoM single-collector (SC-)ICP-MS was used to directly measure both the 71 and 91 mass peaks and their potential isobaric and doubly-charged interferences, during ablation of the Durango apatite. Peaks of 13million and 776 cps were measured for $^{40}Ca^{31}P^{+}$ and $^{44}Ca^{31}P^{16}O^{+}$ respectively, equating to a $^{40}Ca^{31}P^{16}O^{+}/^{40}Ca^{31}P^{+}$ oxide production rate of c.0.3%. These levels of oxide production are essentially identical to those measured by aspirating a U solution suggesting that monitoring of the UO^{+}/U^{+} ratio by solution aspiration is a reasonable proxy during LA-MC-ICP-MS for the levels of Ca-P-O likely to be produced. Therefore, tuning the mass spectrometer and set-up to reduce the UO^{+}/U^{+} levels (and therefore the oxide generation potential of the plasma) by an order of magnitude would be expected to result in a similar reduction in the amount of Ca-P-O produced. Compared to the levels of $^{87}Sr/^{86}Sr$ inaccuracy reported here before calibration (*c*.0.03-0.4%), this would still result in inaccuracies of up to 0.04% for low Sr concentration calcium phosphate samples such as those analysed here. Therefore, when analysing calcium phosphate samples with <~200ppm Sr by LA-ICP-MS, it is unlikely that oxide levels could be reduced to a level whereby all $^{87}Sr/^{86}Sr$ inaccuracy is eliminated. This strongly suggests that direct determination of the oxide interference using SC-ICP-MS, or a daily calibration of the $^{40}Ca^{31}P^{16}O$ interference using a set of reference materials as shown in this study using MC-ICP-MS, is required to achieve accurate $^{87}Sr/^{86}Sr$ ratios on unknowns. In light of this, and the number and level of corrections being applied, the use of secondary reference materials of known isotope ratio, run as unknowns, is considered essential so that accuracy can be demonstrated with each analytical session.

Also of note is the analytical equivalence shown in this study between the human tooth enamel and Durango apatite. This suggests that a series of well

characterised inorganic (and perhaps therefore synthetic) apatites, could be used as calibration materials for biogenic phosphate unknowns. It should also be noted that during LA-ICP-MS analysis of low Ca concentration or Ca-absent phosphate materials, an $^{40}Ar^{31}P^{16}O$ polyatomic may be as problematic as the $^{40}Ca^{31}P^{16}O$ interference shown here. Due to the equivalent isotopic abundance of ^{40}Ca and ^{40}Ar, and the stoichiometric abundance of Ca in the materials used here, discrimination between these two species (if both are present) is not required.

5.2 The $^{87}Sr/^{86}Sr$ isotope composition of the Ferry Fryston cattle tooth

The methodology was applied to analyses of a cattle molar taken from a pit containing a large deposit of cattle bones (c. 250 animals), excavated in the parish of Ferry Fryston, Yorkshire, England NGR SE 4469 4255 (Brown et al. 2007). The site was located on the Magnesian Limestone ridge that runs roughly north-south and comprised an Iron Age square barrow with a male skeleton buried with a chariot and an encircling pit containing the cattle remains. Although radiocarbon dating indicates the centrally buried male died in the 4th to 2nd century BC, dates from the cattle bones suggest they were deposited in the 2nd to 4th centuries AD (Brown et al. 2007) and are, therefore, not contemporary with the chariot burial.

The LA $^{87}Sr/^{86}Sr$ ratios from the cusp to the cervix of the cattle third molar show a progressive increase from 0.7158 to 0.7185 (Figure 6d). A very similar range of ratios from 0.7153 to 0.7183 were obtained from transverse enamel sections analysed by TIMS. All these values are very different to that of the Magnesian Limestone from which the tooth was excavated, i.e. ≤0.7086 (McArthur et al. 2001). The last LA and TIMS analyses suggest the $^{87}Sr/^{86}Sr$ ratio is falling in the final cervical enamel. This could be evidence for the animal being moved to a less

radiogenic biosphere, e.g. limestone pasture shortly before death. However, the cervical enamel at this sampling site was still mineralising at the time of death and diagenetic alteration by the limestone, as is the case for the tooth dentine which gave $^{87}Sr/^{86}Sr = 0.7137$, cannot be ruled out for this sample. Enamel $^{87}Sr/^{86}Sr$ values >0.715 are considerably more radiogenic than any values currently published for animals or humans excavated from the biospheres overlying the Cenozoic, Mesozoic and upper Palaeozoic sedimentary lithologies of England. They are also only rarely found in European studies, where they are attributed to a granitic source (e.g. Price et al. 2004; Price & Gestdottir 2006; Bentley & Knipper 2005; Bentley et al. 2004; Schweissing & Grupe 2003). One reason for this is the greater influence of soluble non-radiogenic carbonate minerals, and in maritime islands such as Britain, rainwater, on dietary $^{87}Sr/^{86}Sr$ in biospheres overlying more radiogenic terrains (Montgomery et al. 2007). The cusp to cervix shift is large and highly significant, indicating a change, or changes, in the source of dietary strontium during the year the third molar crown was mineralizing. The direction of change is opposite to that which might be expected if the animal moved from a radiogenic biosphere to an area of lower values such as Yorkshire. It is possible, therefore, that the animal was slaughtered soon after arrival in the Ferry Fryston area and did not have time to assimilate less radiogenic $^{87}Sr/^{86}Sr$ feed that would have caused a reduction on the $^{87}Sr/^{86}Sr$ values in its third molar enamel profile.

6. CONCLUSIONS

A ^{40}Ca-^{31}P dimer and ^{40}Ca-^{31}P-^{16}O polyatomic ion are generated in the inductively coupled plasma during LA-ICP-MS analysis of calcium phosphate matrices. The amount of this polyatomic ion produced is proportional to the amount

of Ca and P being introduced during ablation and the amount of oxide being generated in the plasma. The polyatomic ion has a dominant mass of 87 and so directly interferes on ^{87}Sr, preventing the accurate determination of $^{87}Sr/^{86}Sr$ ratios in samples with Sr concentrations <~1000ppm. Our data indicate that it is not possible to reduce the oxide generation potential of the plasma sufficiently to completely eliminate formation of this polyatomic ion. However, once corrections for doubly-charged REE's, Ca dimers and Rb interferences have been made (in that order), the remaining inaccuracy in $^{87}Sr/^{86}Sr$ ratios can be calibrated, using a set of reference materials characterised for their Sr isotope ratios. Inorganic or even synthetically generated calcium phosphates (i.e igneous or laboratory grown apatites) could likely be used for this purpose. After correction for the Ca-P-O interference, the resulting data are more accurate, as validated using TIMS, although the uncertainties on the laser ablation data for samples with concentrations of ~100-200ppm Sr are still relatively large.

Currently therefore, the limiting uncertainty for $^{87}Sr/^{86}Sr$ data generated using LA-MC-ICP-MS from archaeological phosphate samples with <~200ppm Sr, is ~0.1-0.2% (2σ). For samples with Sr concentrations ~300ppm, uncertainties of c.0.05% can be achieved. The corrections required and signal levels described, are very small but are shown to be crucial to data quality. This is especially so for $^{84}Sr/^{86}Sr$ ratios where very small 84 beams (on the order of ~200,000 cps) include a large proportion of a Ca dimer which must be corrected to maintain this monitor of correction accuracy and data quality. For high Sr samples, uncertainties of *c.*0.02% 2SD can be achieved where the Ca-P-O correction proves largely insignificant.

This new methodology was applied to a TIMS-characterised cattle tooth excavated from a site in the north of England. The enamel of this Ferry Fryston cattle tooth has a radiogenic signature ($^{87}Sr/^{86}Sr$ = 0.715-0.718) that contrasts with the

$^{87}Sr/^{86}Sr$ isotope signature of the area in which it was found, restricting its possible origins to areas of old and/or radiogenic rocks that are of only restricted occurrence in Britain. It is likely therefore, that this animal was slaughtered shortly after moving from its original location before the less radiogenic Sr signature representing its new location had time to become established in the enamel structure.

Acknowledgements. Thanks to Nick Pearce, University of Wales Aberystwyth, for providing apatite sample 326333 and to Melanie Leng for the mollusc shell. We are grateful to Jon Patchett, Randy Parrish and Geoff Nowell for commenting on early versions of this manuscript and to Angela Boyle at Oxford Archaeology for providing the cattle teeth from the Ferry Fryston chariot burial. Two anonymous reviewers and the review and editorial handling of Clark Johnson are gratefully acknowledged. This study was supported by NIGFSC grant number IP/715/1001.

Table & Figure captions

Table 1 – TIMS data for tooth calibration samples and Ferry Fryston cattle tooth

Table EA1 – MC-ICP-MS and laser ablation system set-up parameters

Table 2a – Collector configuration using the U-Pb block on the Nu Plasma HR. Figures in bold are the key half-mass peaks for correction of REE^{2+}

Table 2b – Table of analyte isotopes and their interferences. Figures in bold are the key half-mass peaks for correction of REE^{2+}

Table EA2 – REE and Ca isotope ratios used in the corrections. All ratios taken from Rosman and Taylor (1998)

Table 3a – LA-MC-ICP-MS data for daily Ca-P-O calibration of Figure 3a

Table 3b – LA-MC-ICP-MS data for Ferry Fryston cattle tooth

Table EA3 – LA-MC-ICP-MS data for calibration materials collected over various sessions, to demonstrate size of peak intensities, size and correction of interferences and final corrected stable isotope ratios.

Fig.1a – $^{87}Sr/^{86}Sr$ data for carbonate shell over the period of analysis; reproducibility of all data is ± 137ppm, 2SD.

Fig 1b. – $^{84}X/^{86}Sr$ of mollusc shell before and after REE^{2+} and Ca_2 corrections; uncertainties are 2SE; final corrected data = 0.05630 ± 0.30% 2SD (dashed line). For comparison, ranges A & B show approximate range of data of Woodhead et al (2005) for marine mollusc shell before and after correction for Ca_2 respectively. Bold line = accepted $^{84}Sr/^{86}Sr = 0.0565$.

Figure 2a - $^{84}X/^{86}Sr$ of Durango apatite before and after REE^{2+} and Ca_2 corrections; uncertainties are 2SE; final corrected data = 0.05643 ± 0.73% 2SD (dashed line).

Figure 2b - $^{87}X/^{86}Sr$ of Durango apatite before and after REE^{2+} and Ca_2 corrections; uncertainties are 2SE; final corrected data = 0.70683 ± 0.032% 2SD (dashed line); TIMS value = 0.706327 (solid line).

Figure 3a – $^{87}Sr/^{86}Sr$ inaccuracy with measured Sr signal

Figure 3b – corrected $^{87}Sr/^{86}Sr$ for apatite 326333; final corrected data = 0.702953 ± 0.0195% 2SD; TIMS value = 0.70296

Figure 4a – Variation of Ca-P-O calibration regression over a number of analytical sessions

Figure 4b – Self-normalised calibration plot to show uncertainty distribution

Figure 4c – Daily reproducibility of tooth calibration materials defining uncertainty propagation function

Figure 5a – $^{84}X/^{86}Sr$ data for carbonate shell, Durango apatite and tooth calibration materials before and after correction for REE^{2+} and Ca_2

Figure 5b –$^{84}Sr/^{86}Sr$ for carbonate shell, Durango apatite and tooth calibration materials after correction for REE^{2+} and Ca_2

Figure 6a – Daily Ca-P-O calibration for Ferry Fryston data

Figure 6b – $^{84}X/^{86}Sr$ for Ferry Fryston cattle tooth before and after correction for REE^{2+} and Ca_2

Figure 6c – All $^{87}X/^{86}Sr$ data for Ferry Fryston cattle tooth

Figure 6d – $^{87}Sr/^{86}Sr$ TIMS data and corrected and propagated $^{87}Sr/^{86}Sr$ LA data for Ferry Fryston cattle tooth

References

Beard B.L. and Johnson C.M. (2000). Strontium isotope composition of skeletal material can determine the birth place and geographic mobility of humans and animals. *Jour. Forensic Sci.,* **45**(5), 1049-1061.

Bentley R.A. 2006. Strontium isotopes from the earth to the archaeological skeleton: A review. *Journal of Archaeological Method and Theory*. **13**,135-187.

Bentley R. A. and Knipper C. (2005). Transhumance at the early Neolithic settlement at Vaihingen (Germany). *Antiquity* **79**(306),

Bentley R. A., Price T. D. and Stephan E. (2004). Determining the 'local' Sr-87/Sr-86 range for archaeological skeletons: a case study from Neolithic Europe. *Journal of Archaeological Science* **31**(4), 365-375.

Birck J. L. (1986). Precision K-Rb-Sr Isotopic Analysis - Application to Rb-Sr Chronology. Chemical Geology, 56(1-2): 73-83.

Bizzarro M., Simonetti A., Stevenson R.K. and Kurszlaukis S. (2003). In situ $^{87}Sr/^{86}Sr$ investigation of igneous apatites and carbonates using laser ablation MC-ICP-MS. *Geochimica et Cosmochimica Acta*, **67**, 2, 289-302.

Bocherens H., Brinkman D. B., Dauphin Y. and Mariotti A. (1994). Microstructural and geochemical investigations on Late Cretaceous archosaur teeth from Alberta, Canada. *Canadian Journal of Earth Sciences* **31,** 783-792.

Brown, F., Howard-Davis, C., Brennand, M., Boyle, A., Evans, T., O'Connor, S., Spence, A., Heawood, R. and Lupton, A. (2007). *The Archaeology of the A1 (M) Darrington to Dishforth DBFO Road Scheme*. Lancaster: Oxford Archaeology North.

Budd P., Montgomery J., Barreiro B. and Thomas R. G. (2000). Differential diagenesis of strontium in archaeological human dental tissues. *Applied Geochemistry* **15**, 687-694.

Charlier B. L. A., Ginibre C., Morgan D., Nowell G. M., Pearson D. G., Davidson J. P. and Otley C. J. (2006). Methods for the microsampling and high-precision analysis of strontium and rubidium isotopes at single crystal scale for petrological and geochronological applications. *Chemical Geology*, **232**, 114-133.

Dauphin Y. and Williams C. T. (2004). Diagenetic trends of dental tissues. *Comptes Rendus Palevol* **3**, 583-590.

Davidson J., Tepley. F., Palacz Z. and Meffan-Main S. (2001). Magma recharge, contamination and residence times revealed by in situ laser ablation isotopic analysis of feldspar in volcanic rocks. *Earth and Planetary Science Letters*, **184**, 427-442

Guillong M. and Günther D. (2002). Effect of particle size distribution on ICP-induced elemental fractionation in laser ablation-inductively coupled plasma-mass spectrometry. *Journal of Analytical Atomic Spectrometry* **17**, 831-837.

Hoppe K. A., Koch P. L. and Furutani T. T. (2003). Assessing the preservation of biogenic strontium in fossil bones and tooth enamel. *International Journal of Osteoarchaeology* **13**, 20-28.

Horn P., Hölzl S. and Storzer D. (1994). Habitat determination on a fossil stag's mandible from the site of Homo erectus heidelbergensis at Mauer by use of $^{87}Sr/^{86}Sr$. *Naturwissenschaften* **81**, 360-362.

Horstwood M.S.A. and Evans J.A. (2002). Complications of LA-MC-ICP-MS Sr isotope analysis of phosphate matrices. 8th International Conference on Plasma Source Mass Spectrometry. University of Durham, UK, 8th-13th September 2002.

Horstwood M. S. A. and Nowell G. M. (2005) Multi-collector devices. In: *ICP-MS Handbook*, (ed. Nelms S.) Blackwell Publishing. pp.54-68

Koch P. L., Tuross N. and Fogel M. (1997). The effects of sample treatment and diagenesis on the isotopic integrity of carbonate in biogenic hydroxylapatite. *Journal of Archaeological Science* **24**, 417-429.

McArthur J. M., Howarth R. J. and Bailey T. R. (2001). Strontium isotope stratigraphy: LOWESS version 3: best fit to the marine Sr-isotope curve for 0-509 Ma and accompanying look- up table for deriving numerical age. *Journal of Geology* **109**(2), 155-170.

Michel V., Ildefonse P. and Morin G. (1996). Assessment of archaeological bone and dentine preservation from Lazaret Cave (Middle Pleistocene) in France. *Palaeogeography, Palaeoclimatology, Palaeoecology*. **126**, 109-119.

Montgomery J. (2002). Lead and Strontium Isotope Compositions of Human Dental Tissues as an Indicator of Ancient Exposure and Population Dynamics. PhD thesis, University of Bradford, UK.

Montgomery J., Evans J. A. and Cooper R. E. (2007). Resolving archaeological populations with $^{87}Sr/^{86}Sr$ mixing diagrams. *Applied Geochemistry* **22**, 1502-1514.

Nowell G. M., Pearson, D.G., Parman, S.W., Luguet, A. and Hanski, E. (2007). Precise and accurate 186Os/188Os and 187Os/188Os measurements by Multi-Collector Plasma Ionisation Mass Spectrometry, part II: Laser ablation and its application to single-grain Pt-Os and Re-Os geochronology. *Chemical Geology*, **248**, 394-426

Paton C., Woodhead J., Hergt J., Phillips D. and Shee S. (2007). Sr-isotope analysis of kimberlitic groundmass perovskite via LA-MC-ICP-MS. *Geostandards and Geoanalytical Research*, **31,** no.4, 321-330

Pearce, N.J.G., and Leng, M.J. (1996). The origin of carbonatites and related rocks from the Igaliko Dyke Swarm, Gardar Province, South Greenland: field, geochemical and C-O-Sr-Nd isotope evidence. *Lithos*, **39**, Iss.1-2, 21-40.

Price T. D. and Gestsdottir H. (2006). The first settlers of Iceland: an isotopic approach to colonisation. *Antiquity* **80**, 130-144.

Price T. D., Knipper C., Grupe G. and Smrcka V. (2004). Strontium isotopes and prehistoric human migration: the Bell Beaker Period in Central Europe. *European Journal of Archaeology* **7**(1), 9-40.

Prohaska T., Latkoczy C., Schultheis G., Teschler-Nicola M. and Stingeder G. (2002). Investigation of Sr isotope ratios in prehistoric human bones and teeth using laser ablation ICP-MS and ICP-MS after Rb/Sr separation. *Journal of Analytical Atomic Spectrometry* **17**, 887-891.

Ramos F. C., Wolff J. A. and Tollstrup D. L. (2004). Measuring 87Sr/86Sr variations in minerals and groundmass from basalts using LA-MC-ICP-MS. *Chemical Geology*, **211**, 135-158

Richards M., Harvati K., Grimes V., Smith C., Smith T., Hublin J-J., Karkanas P. and Panagopoulou E. (2007). Strontium isotope evidence of Neanderthal mobility at the site of Lakonis, Greece using laser-ablation PIMMS. *Journal of Archaeological Science*, **vol**, 1-6

Rink W. J. and Schwarcz H. P. (1995). Tests for Diagenesis in Tooth Enamel: ESR Dating Signals and Carbonate Contents. *Journal of Archaeological Science* **22**, 251-255.

Rosman K. J. R. and Taylor P. D. P. (1998). Isotopic composition of the elements 1997. *Pure and Applied Chemistry*, **70**(1), 217-235

Schmidtberger S. S. Simonetti A. and Francis D. (2003). Small-scale Sr isotope investigation of clinopyroxenes from peridotite xenoliths by laser ablation MC-ICP-MS – implications for mantle metasomatism. *Chemical Geology*, **199**, 317-329

Schweissing M. M. and Grupe G. (2003). Stable strontium isotopes in human teeth and bone: a key to migration events of the late Roman period in Bavaria. *Journal of Archaeological Science* **30**, 1373-1383.

Simonetti A., Buzon M.R. and Creaser R.A. (2007) Elemental and Sr isotope investigations of human tooth enamel by laser ablation-(MC)-ICP-MS: Successes and pitfalls. *Geochimica et Cosmochimica Acta*, **71**, Iss.15, Supp.1, A940

Simonetti A., Buzon M.R. and Creaser R.A (2008) In-Situ Elemental And Sr Isotope Investigation Of Human Tooth Enamel By Laser Ablation-(MC)-ICP-MS: Successes And Pitfalls. *Archaeometry*, **50**, 2, 371-385

Smith C. E. (1998). Cellular and chemical events during enamel maturation. *Critical Reviews in Oral Biology and Medicine* **9**, 128-161.

Trotter J. A. and Eggins S. M. (2006). Chemical systematics of conodont apatite determined by laser ablation ICPMS. *Chemical Geology*, **233**, 196-216

Trickett M. A., Budd P., Montgomery J. and Evans J. (2003). An assessment of solubility profiling as a decontamination procedure for the Sr-87/Sr-86 analysis of archaeological human skeletal tissue. *Applied Geochemistry* **18**, 653-658.

Waight T., Baker J. and Peate D. (2002). Sr isotope ratio measurements by double-focussing MC-ICPMS: techniques, observations and pitfalls. *International Journal of Mass Spectrometry*, **221**, 229-244

Wang Y. and Cerling T. E. (1994). A model of fossil tooth and bone diagenesis: implications for paleodiet reconstruction from stable isotopes. *Palaeogeography, Palaeoclimatology, Palaeoecology* **107**, 281-289.

Woodhead J., Swearer S., Hergt J. and Maas R. (2005). In situ Sr-isotope analysis of carbonates by LA-MC-ICP-MS: interference corrections, high spatial

resolution and an example from otolith studies. *Journal Analytical Atomic Spectrometry*, **20**, 22-27

Figures

Figure 1a

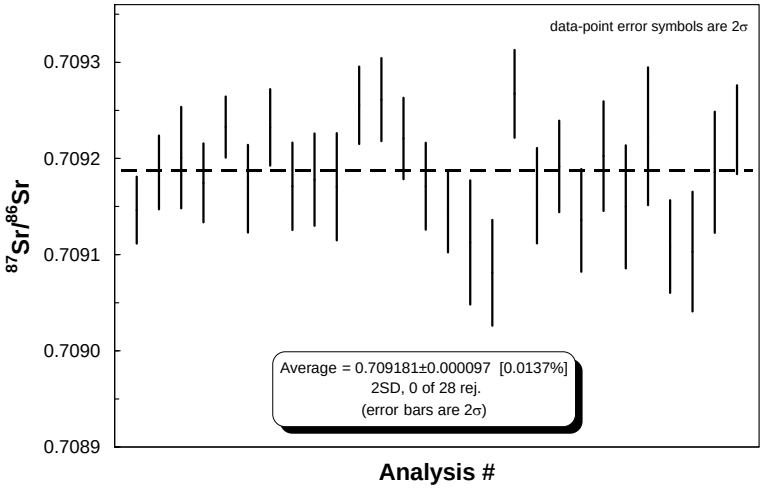

Figure 1b

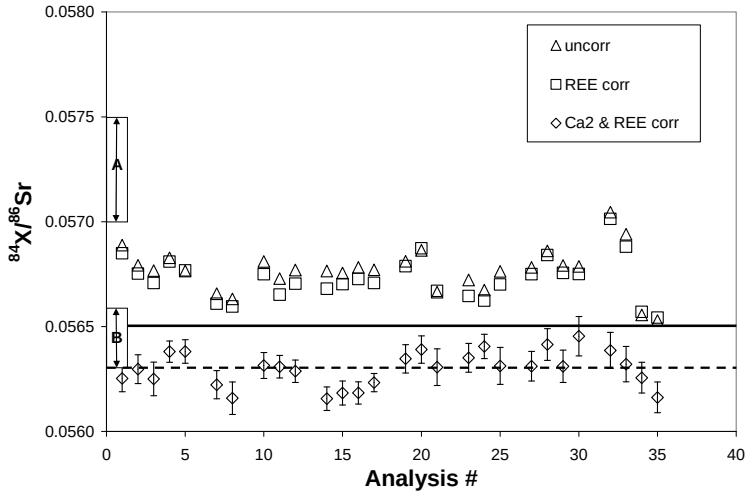

Figure 2a

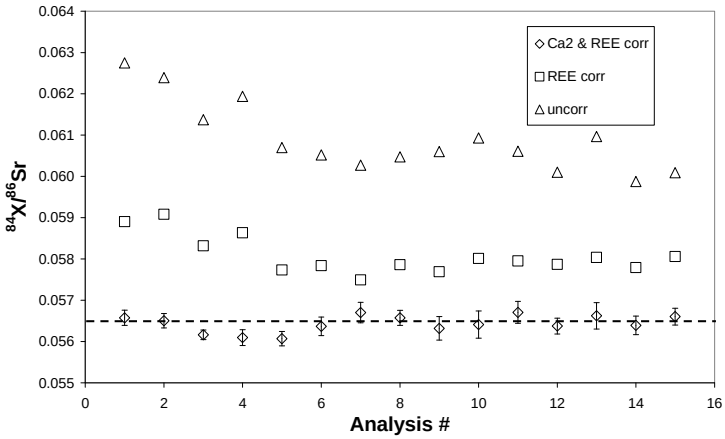

Figure 2b

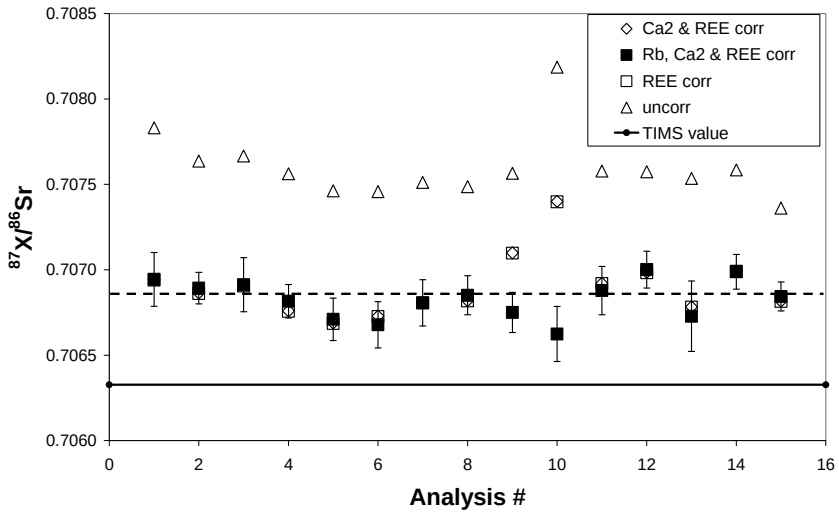

Figure 3a

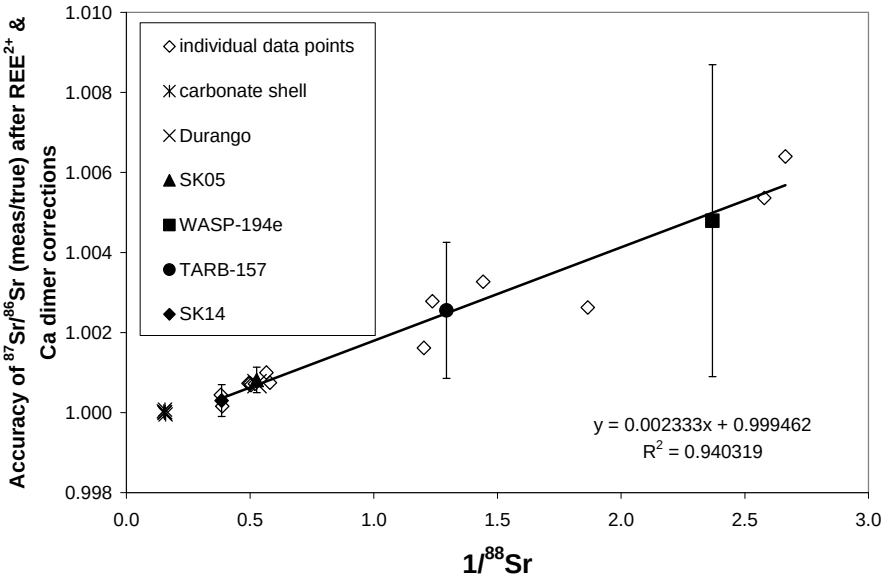

Figure 3b

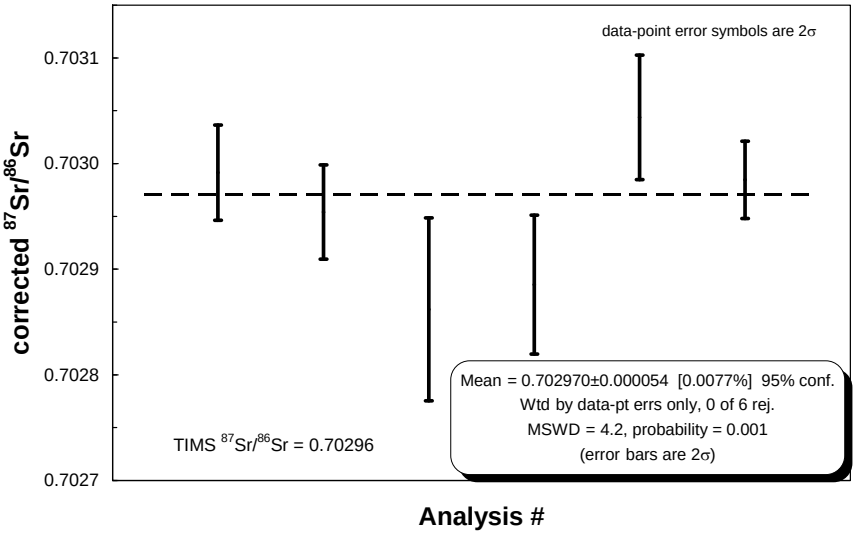

Figure 4a

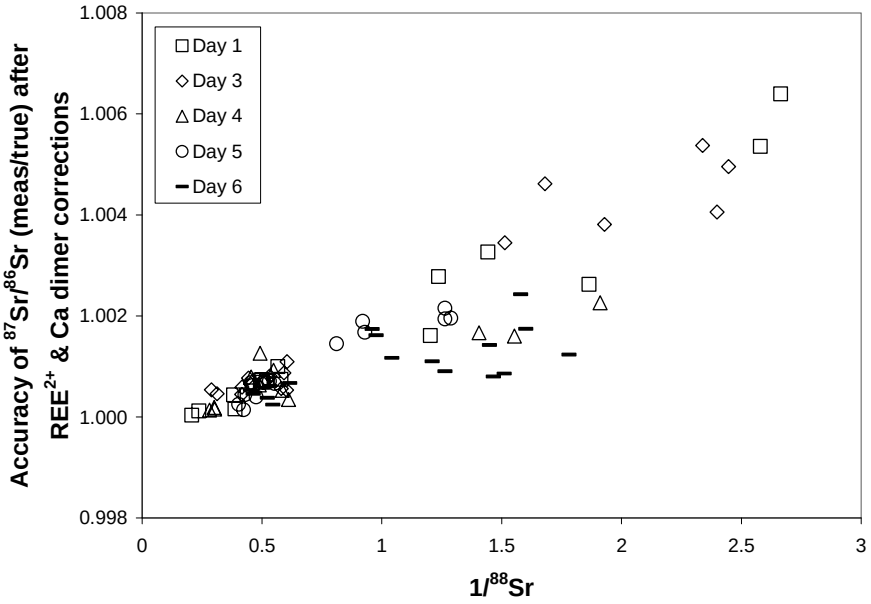

Figure 4b

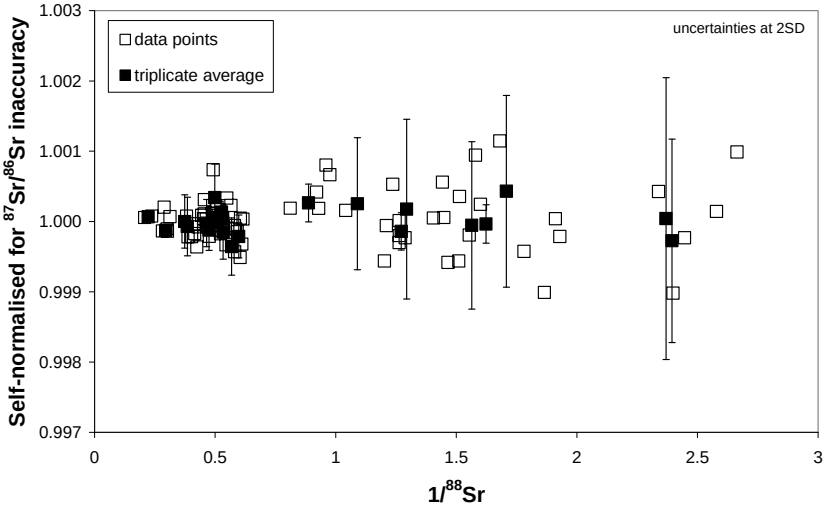

Figure 4c

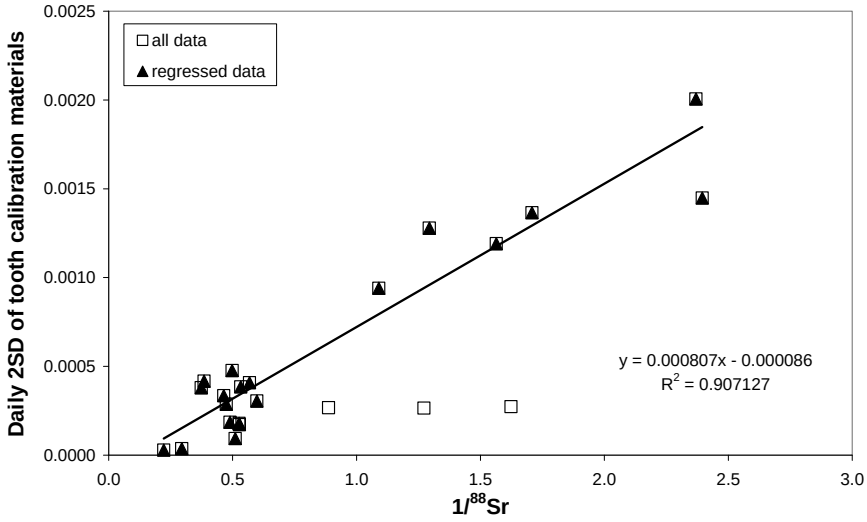
Daily 2SD of tooth calibration materials
1/88Sr
all data
regressed data
y = 0.000807x - 0.000086
R2 = 0.907127
0.0025
0.0020
0.0015
0.0010
0.0005
0.0000
0.0
0.5
1.0
1.5
2.0
2.5
3.0

Figure 5a

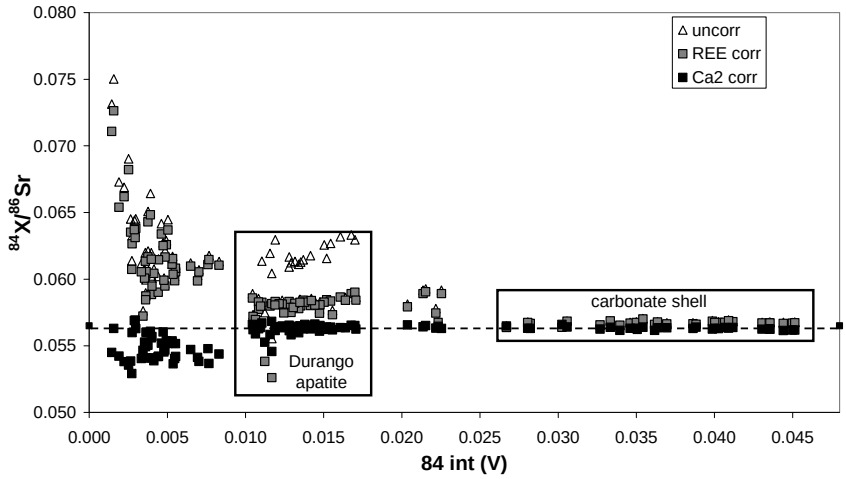

Figure 5b

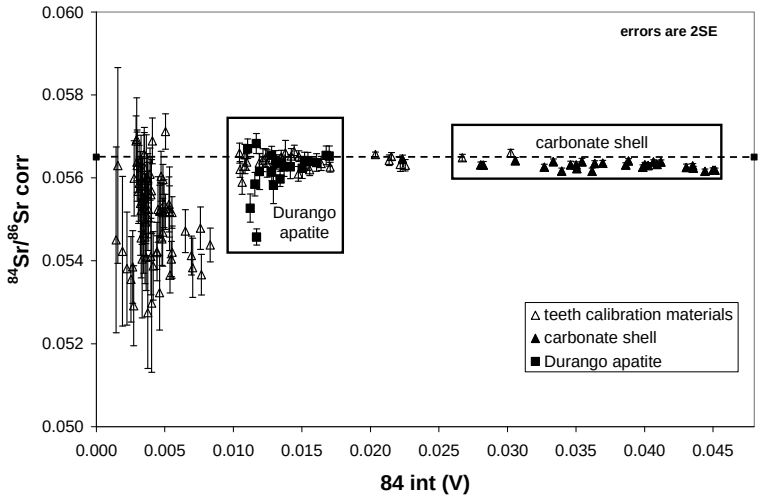

Figure 6a

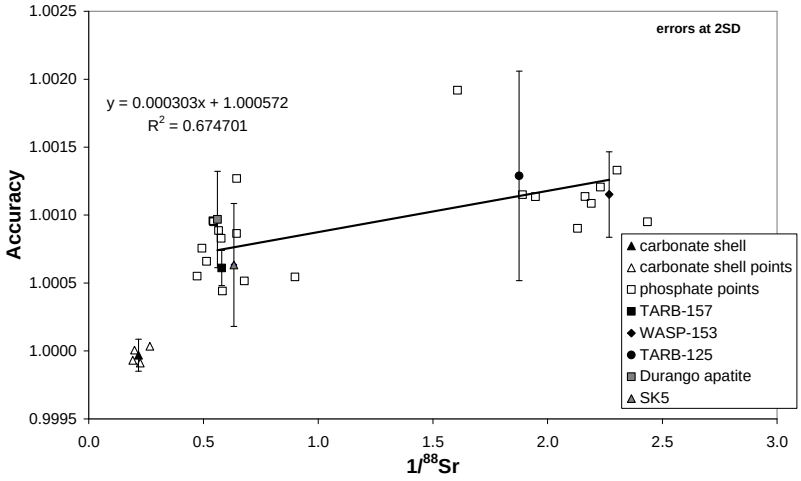

Figure 6b

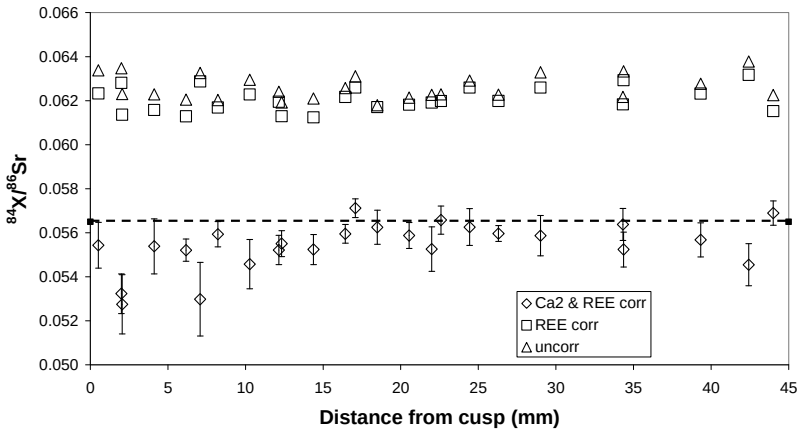

Figure 6c

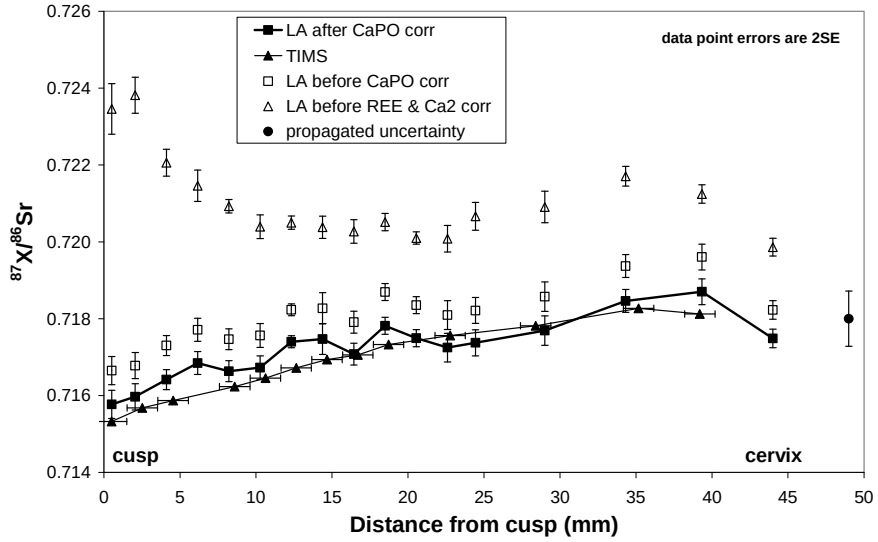

Figure 6d

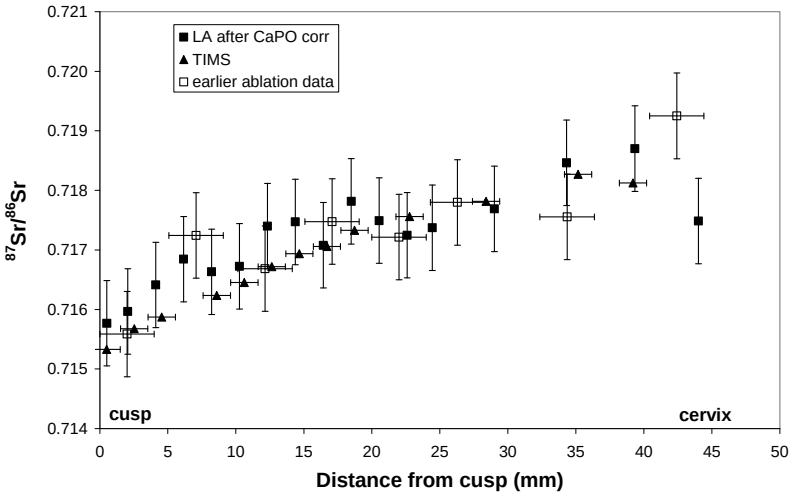

Tables

Table 1 - TIMS data for tooth calibration samples & Ferry Fryston Cattle Tooth

sample	Sr ppm	$^{87}Sr/^{86}Sr$"	Distance from cusp# (mm)
WASP-153e	90	0.710719	N/A
WASP-194e	103	0.710634	N/A
TARB-125	142	0.711012	N/A
TARB-157	185	0.709927	N/A
SK014	264	0.709494	N/A
SK005	373	0.709456	N/A
Durango apatite	462*	0.706327	N/A
apatite 326333	c. 35,000$	0.702960	N/A
FBCT-5A	158	0.715328	0.5
FBCT-5B	151	0.715679	2.5
FBCT-5C	163	0.715871	4.6
FBCT-5E	153	0.716234	8.6
FBCT-5F	165	0.716455	10.6
FBCT-5G	169	0.716720	12.7
FBCT-5H	173	0.716937	14.7
FBCT-5I	179	0.717057	16.7
FBCT-5J	184	0.717331	18.7
FBCT-5L	197	0.717562	22.8
FBCT-5N	196	0.717816	28.4
FBCT-5Q	218	0.718271	35.2
FBCT-5S	169	0.718125	39.2

uncertainty +/- 1mm

" Internal precision <0.001% (2SE) for all samples; heterogeneity assumed to be <~0.005% (Montgomery (2002))

* Trotter & Eggins 2006

$ Pearce & Leng 2006

$^{87}Sr/^{86}Sr$ of modern mollusc assumed to reflect seawater composition of 0.70918

Table EA1 – MC-ICP-MS and laser ablation system set-up parameters

MC-ICP-MS	Nu Plasma HR (Nu Instruments) – fitted with U-Pb collector block
Nebuliser	DSN-100 + ESI PFA-50 connected to sample line via T-connector
Neb flow	25psi/~0.7l/min
Aspirated solution	blank acid (2% HNO3) during analysis
Hot gas flow	0.16l/min
Sweep gas flow	c.4.5l/min
Uptake rate	c.70ul/min
Carrier gas	He @800ul/min
Torch-cone distance	~10-12mm
Cool flow	13l/min
Auxilary flow	0.8l/min
RF forward power	1500W with 0W reflected
Sampling cone	Ni
Skimmer cone	Ni with 0.7mm orifice
Detectors	all Faraday
Solution standard	NBS987
UO+/U+	~0.25-1%
Laser	UP193SS Nd:YAG (New Wave Research)
Wavelength	193nm
Fluence	c.8J/cm^2 - output fluence used; independently calibrated at sample surface
Pulse width	c.3ns
Rep rate	10Hz
Cell volume	~30cm3
spot size	100um
Ablation protocol	260x350um box raster
Raster spacing	90um
Scan speed	30um/sec
Z-focus change per raster pass	none
Ablation standard	mollusc shell carbonate and high Sr igneous apatite

Table 2a - Collector configuration using the Nu Plasma HR

	H4	H3	H2	H1	Ax	L1	L2	Integ'n. time (secs)
Seq 1	84	**83.5**	83	82.5	82	**81.5**	81	3
Seq 2	86	**85.5**	85	84.5	84	**83.5**	83	3
Seq 3	88	87.5	87	**86.5**	86	85.5	85	3

Table 2b – Table of analyte isotopes and their interferences

89	88	87.5	87	86.5	86	85.5	85	84.5	84	83.5	83	82.5	82	81.5	81
	Sr		Sr		Sr				Sr						
			Rb				Rb								
					Kr				Kr		Kr		Kr		
Y	Lu^{2+}	Lu^{2+}	Yb^{2+}	**Yb^{2+}**	Yb^{2+}	**Yb^{2+}**	Yb^{2+} Er^{2+}	Tm^{2+}	Yb^{2+} Er^{2+}	**Er^{2+}**	Er^{2+}	Ho^{2+}	Er^{2+} Dy^{2+}	**Dy^{2+}**	Ar_2H
	$^{40}Ca^{48}Ca$				$^{40}Ca^{46}Ca$				$^{40}Ca^{44}Ca$				$^{40}Ca^{42}Ca$		
			$^{40}Ca^{31}P^{16}O$												

Table EA2 - REE and Ca isotope ratios used in corrections	
$^{173}Yb/^{171}Yb$	1.129552
$^{171}Yb/^{172}Yb$	0.654146
$^{173}Yb/^{174}Yb$	0.506755
$^{173}Yb/^{172}Yb$	0.738891
$^{173}Yb/^{170}Yb$	5.30592
$^{173}Yb/^{176}Yb$	1.26411
$^{167}Er/^{168}Er$	0.856236
$^{167}Er/^{166}Er$	0.682237
$^{167}Er/^{164}Er$	14.24224
$^{163}Dy/^{164}Dy$	0.883605
$^{44}Ca/^{42}Ca$	3.22411
$^{46}Ca/^{42}Ca$	0.00618
$^{44}Ca/^{40}Ca$	0.021518

Table 3a - LA-MC-ICP-MS data for daily Ca-P-O calibration of Figure 3a

Peak intensities

Sample	^{88}Total	^{87}Total	^{86}Total	^{84}Total	^{85}Rb$^+$	^{163}Dy^{2+} (81.5)	^{175}Lu^{2+} (87.5)	^{173}Yb^{2+} (86.5)	^{171}Yb^{2+} (85.5)	^{167}Er^{2+} (83.5)	mass bias	1se
LoD (3SD)	2.07E-04	2.12E-05	4.32E-05	1.78E-04	6.00E-05	4.64E-05	4.79E-05	3.04E-05	6.67E-05	3.34E-05		
Wall	8.33E+00	5.29E-01	3.07E-05	3.96E-02	1.27E-04	3.47E-05	-2.73E-05	2.11E-05	2.23E-05	4.80E-05	0.99129	0.00002
Wall	8.41E+00	5.32E-01	5.11E-05	4.03E-02	9.74E-05	2.97E-05	-1.33E-05	1.46E-05	2.05E-05	4.09E-05	0.99139	0.00002
Wall	8.82E+00	5.59E-01	4.05E-05	4.30E-02	1.06E-04	2.86E-05	-2.74E-05	5.27E-06	6.45E-06	4.55E-05	0.99092	0.00002
Wall	8.51E+00	5.41E-01	3.24E-05	4.12E-02	9.67E-05	3.57E-05	-1.80E-06	9.47E-06	1.41E-05	1.63E-05	0.99124	0.00005
Wall	8.42E+00	5.33E-01	2.61E-05	4.07E-02	8.57E-05	2.28E-05	-3.70E-06	1.10E-05	8.75E-06	1.73E-05	0.99114	0.00003
Durango	2.00E+00	1.88E-01	4.55E-04	1.35E-02	1.19E-04	1.44E-03	8.79E-05	1.85E-04	1.89E-04	8.47E-04	0.99157	0.00004
Durango	1.72E+00	1.43E-01	4.49E-04	1.16E-02	1.22E-04	1.44E-03	8.51E-05	1.87E-04	1.55E-04	8.51E-04	0.99185	0.00005
Durango	1.99E+00	1.85E-01	4.59E-04	1.34E-02	1.25E-04	1.41E-03	8.16E-05	1.81E-04	1.89E-04	8.37E-04	0.99234	0.00003
SK35	1.77E+00	1.40E-01	7.60E-04	1.06E-02	8.99E-05	5.54E-05	2.56E-05	2.27E-05	4.85E-05	4.93E-05	0.99279	0.00003
SK35	1.82E+00	1.81E-01	5.14E-04	1.25E-02	7.19E-05	5.48E-05	1.47E-05	2.04E-05	4.85E-05	4.01E-05	0.99253	0.00004
SK35	2.03E+00	1.89E-01	8.67E-04	1.31E-02	1.01E-04	4.47E-05	2.56E-05	3.88E-05	4.45E-05	5.47E-05	0.99252	0.00002
WASP-19a	5.38E-01	4.83E-02	1.50E-03	3.77E-03	1.23E-04	5.13E-05	1.82E-05	2.47E-05	3.75E-05	3.86E-05	0.99184	0.00006
WASP-19a	3.68E-01	3.27E-02	4.14E-04	2.73E-03	1.09E-04	3.48E-05	1.43E-05	2.17E-05	3.53E-05	2.15E-05	0.99232	0.00010
WASP-19a	3.75E-01	3.19E-02	2.97E-04	2.65E-03	1.32E-04	3.12E-05	4.29E-07	1.60E-05	3.74E-05	4.29E-05	0.99230	0.00010
TARB-157	6.63E-01	5.84E-02	1.05E-03	4.85E-03	1.18E-04	4.61E-05	8.04E-06	4.54E-06	2.74E-05	1.67E-05	0.99237	0.00005
TARB-157	8.09E-01	6.89E-02	1.25E-03	4.78E-03	1.50E-04	3.98E-05	1.13E-05	1.64E-05	4.09E-05	2.15E-05	0.99190	0.00006
TARB-157	8.32E-01	6.89E-02	1.39E-03	5.62E-03	1.06E-04	4.03E-05	1.72E-05	1.60E-05	2.51E-05	3.01E-05	0.99233	0.00003
SK14	2.59E+00	2.15E-01	4.70E-04	1.64E-02	1.76E-04	5.27E-05	4.81E-06	4.88E-05	2.63E-05	5.60E-05	0.99155	0.00003
SK14	2.82E+00	2.19E-01	5.91E-04	1.71E-02	1.99E-04	7.68E-05	1.48E-05	5.83E-05	4.64E-05	6.34E-05	0.99189	0.00006

Sample	^{84}Sr/^{86}Sr ratios: mbc only	1se	REEcorr	1se	Ca/corr	1se	^{87}Sr/^{86}Sr ratios: mbc only	1se	Rb corr only	1se	before CaPO corr	1se	Size of REE^{2+} & Ca$_x$ corr (ppm)	TIMS	Deviation
Wall	0.05989	0.00001	0.05986	0.00001	0.05825	0.00003	0.70917	0.00002	0.70917	0.00002	0.70915	0.00002	42	0.70918	1.000014
Wall	0.05979	0.00001	0.05975	0.00001	0.05830	0.00003	0.70920	0.00002	0.70920	0.00002	0.70919	0.00002	27		
Wall	0.05977	0.00001	0.05971	0.00001	0.05825	0.00004	0.70922	0.00002	0.70922	0.00002	0.70920	0.00002	9		
Wall	0.05983	0.00001	0.05981	0.00001	0.05830	0.00003	0.70923	0.00002	0.70920	0.00002	0.70919	0.00002	17		
Wall	0.05977	0.00001	0.05977	0.00001	0.05830	0.00003	0.70928	0.00001	0.70925	0.00001	0.70923	0.00002	20		
Durango	0.08129	0.00007	0.05800	0.00004	0.05836	0.00009	0.70763	0.00004	0.70763	0.00005	0.70685	0.00036	1085	0.706327	1.000724
Durango	0.08164	0.00009	0.05799	0.00004	0.05885	0.00014	0.70774	0.00005	0.70777	0.00006	0.70685	0.00036	1293		
Durango	0.08112	0.00009	0.05779	0.00005	0.05897	0.00009	0.70762	0.00004	0.70761	0.00004	0.70681	0.00036	1171		
SK35	0.05957	0.00005	0.05773	0.00005	0.05829	0.00009	0.71165	0.00018	0.71031	0.00006	0.71017	0.00037	215	0.709458	1.000817
SK35	0.05763	0.00005	0.05748	0.00005	0.05835	0.00017	0.71093	0.00008	0.71011	0.00006	0.70997	0.00037	199		
SK35	0.05915	0.00004	0.05788	0.00004	0.05845	0.00013	0.71143	0.00007	0.71018	0.00004	0.70997	0.00034	203		
WASP-19a	0.08211	0.00013	0.08167	0.00014	0.05605	0.00043	0.71988	0.00179	0.71291	0.00011	0.71250	0.00013	532	0.710934	1.004790
WASP-19a	0.08138	0.00015	0.08073	0.00016	0.05292	0.00048	0.71929	0.00027	0.71491	0.00016	0.71444	0.00020	583		
WASP-19a	0.08451	0.00014	0.08353	0.00011	0.05395	0.00044	0.71799	0.00029	0.71582	0.00018	0.71518	0.00015	501		
TARB-157	0.05968	0.00009	0.05948	0.00010	0.05499	0.00041	0.71790	0.00058	0.71255	0.00013	0.71225	0.00014	38	0.709927	1.002556
TARB-157	0.08004	0.00009	0.05992	0.00005	0.05453	0.00032	0.71729	0.00022	0.71198	0.00009	0.71190	0.00011	209		
TARB-157	0.08103	0.00009	0.08082	0.00010	0.05617	0.00019	0.71884	0.00012	0.71133	0.00008	0.71107	0.00039	210		
SK14	0.05983	0.00002	0.05941	0.00003	0.05836	0.00008	0.71036	0.00010	0.70977	0.00003	0.70981	0.00034	228	0.709494	1.000301
SK14	0.05985	0.00003	0.05942	0.00003	0.05826	0.00008	0.71071	0.00006	0.71000	0.00004	0.70981	0.00034	243		

bold = above LoD, italic = below LoD

* after correction for REE^{2+} interference

LoD taken as typical daily 3SD of on-peak background

Table 3b - LA-MC-ICP-MS data for Ferry Fryston cattle tooth

	Peak intensities												$^{84}Sr/^{86}Sr$ ratios						$^{87}Sr/^{86}Sr$ ratios								Size of REE^{2+}	Size of
	^{88}Total	^{87}Total	^{85}Total	^{84}Total	$^{83}Ca^{+}$	$^{163}Dy^{2+}$ (81.5)	$^{175}Lu^{2+}$ (87.5)	$^{173}Yb^{2+}$ (86.5)	$^{171}Yb^{2+}$ (85.5)	$^{167}Er^{2+}$ (83.5)													before		after		& Ca_2 corr	CaPO corr
LoD (3SD)	2.07E-04	2.12E-05	4.25E-05	1.70E-04	6.00E-05	4.94E-05	4.78E-05	2.84E-05	5.67E-06	2.24E-05																		
Distance from cusp[#] (mm)											mass bias	1se	mbc only	1se	REEcorr	1se	Ca corr	1se	mbc only	1se	Rb corr only	1se	CaPO corr	1se	CaPO corr	1se	(ppm)	(ppm)
0.8	4.62E-01	3.92E-02	8.86E-04	3.32E-03	1.13E-04	2.57E-05	2.05E-05	1.31E-05	2.40E-05	4.14E-05	0.90207	0.00007	0.06238	0.00016	0.05233	0.00012	0.05544	0.00104	0.72346	0.00033	0.71592	0.00015	0.71565	0.00019	0.71577	0.00018	385	1226
2.1	5.39E-01	4.56E-02	1.11E-03	3.75E-03	1.07E-04	3.44E-05	1.94E-05	1.17E-05	2.29E-05	3.07E-05	0.90213	0.00005	0.06236	0.00008	0.05136	0.00010	0.05215	0.00134	0.72382	0.00023	0.71701	0.00015	0.71578	0.00017	0.71597	0.00017	317	1133
4.1	4.52E-01	3.84E-02	6.31E-04	3.22E-03	9.56E-05	2.85E-05	8.27E-06	1.44E-05	2.06E-05	2.45E-05	0.90218	0.00005	0.06229	0.00016	0.05150	0.00012	0.05538	0.00125	0.72265	0.00018	0.71756	0.00009	0.71730	0.00013	0.71641	0.00013	346	1240
6.2	4.77E-01	4.04E-02	5.23E-04	3.27E-03	1.06E-04	8.08E-06	1.52E-05	1.40E-05	2.26E-05	4.71E-05	0.90203	0.00007	0.06236	0.00008	0.05129	0.00010	0.05521	0.00050	0.72146	0.00020	0.71781	0.00011	0.71771	0.00015	0.71665	0.00015	132	1206
8.2	5.13E-01	4.33E-02	5.06E-04	3.34E-03	9.95E-05	1.74E-05	1.86E-05	1.87E-05	1.69E-05	3.35E-05	0.90216	0.00005	0.06233	0.00012	0.05169	0.00017	0.05594	0.00058	0.72053	0.00035	0.71774	0.00009	0.71747	0.00014	0.71663	0.00014	385	1163
10.3	5.05E-01	4.31E-02	4.36E-04	3.55E-03	1.23E-04	1.69E-05	1.71E-05	2.25E-05	3.00E-05	4.44E-05	0.90290	0.00007	0.06235	0.00013	0.05228	0.00008	0.05457	0.00112	0.72039	0.00016	0.71791	0.00012	0.71756	0.00016	0.71673	0.00015	488	1166
12.3	5.16E-01	4.36E-02	3.91E-04	3.54E-03	1.03E-04	7.03E-06	2.32E-05	2.25E-05	1.52E-05	4.45E-05	0.90286	0.00005	0.06192	0.00013	0.05130	0.00012	0.05501	0.00059	0.72083	0.00035	0.71863	0.00007	0.71822	0.00009	0.71749	0.00009	503	1158
14.4	5.56E-01	4.73E-02	3.31E-04	3.89E-03	1.16E-04	1.80E-05	1.78E-05	2.15E-05	3.21E-05	5.33E-05	0.90203	0.00005	0.06239	0.00013	0.05124	0.00011	0.05524	0.00069	0.72038	0.00014	0.71856	0.00016	0.71827	0.00023	0.71747	0.00023	385	1116
16.4	5.18E-01	4.38E-02	3.35E-04	3.75E-03	1.13E-04	2.77E-05	2.13E-05	1.38E-05	-1.24E-05	4.34E-05	0.90252	0.00005	0.06257	0.00012	0.05217	0.00010	0.05595	0.00042	0.72037	0.00015	0.71815	0.00011	0.71791	0.00014	0.71708	0.00014	332	1155
18.5	4.65E-01	3.93E-02	2.23E-04	3.26E-03	8.85E-05	2.71E-05	1.78E-05	2.01E-05	1.10E-06	4.13E-05	0.90223	0.00008	0.06179	0.00014	0.05171	0.00014	0.05625	0.00077	0.72082	0.00011	0.71902	0.00010	0.71869	0.00011	0.71782	0.00011	405	1222
20.5	4.85E-01	4.10E-02	2.33E-04	3.26E-03	1.01E-04	1.45E-05	1.62E-05	1.32E-05	-5.96E-05	2.24E-05	0.90235	0.00004	0.06214	0.00013	0.05181	0.00010	0.05587	0.00059	0.72013	0.00008	0.71857	0.00008	0.71835	0.00011	0.71749	0.00011	363	1195
22.6	4.98E-01	4.23E-02	2.71E-04	3.49E-03	9.73E-05	2.15E-05	1.48E-05	1.36E-05	-9.67E-05	2.24E-05	0.90244	0.00009	0.06229	0.00016	0.05198	0.00015	0.05557	0.00064	0.72068	0.00017	0.71843	0.00014	0.71859	0.00019	0.71725	0.00019	463	1186
24.4	5.03E-01	4.36E-02	3.21E-04	3.59E-03	1.16E-04	2.39E-05	1.08E-05	2.60E-05	2.57E-06	1.65E-05	0.90265	0.00008	0.06291	0.00013	0.05259	0.00012	0.05528	0.00084	0.72066	0.00018	0.71864	0.00013	0.71821	0.00017	0.71737	0.00017	593	1173
28.0	4.60E-01	3.89E-02	2.45E-04	3.12E-03	1.06E-04	1.27E-05	9.10E-06	1.27E-05	8.55E-06	1.28E-05	0.90213	0.00008	0.06229	0.00013	0.05260	0.00011	0.05507	0.00091	0.72091	0.00021	0.71873	0.00016	0.71857	0.00019	0.71769	0.00019	333	1230
34.3	4.41E-01	3.73E-02	2.41E-04	2.96E-03	8.95E-05	1.30E-05	8.28E-06	1.78E-05	1.75E-06	1.75E-05	0.90256	0.00007	0.06217	0.00014	0.05183	0.00011	0.05538	0.00073	0.72171	0.00013	0.71978	0.00013	0.71937	0.00015	0.71846	0.00015	574	1258
39.3	4.43E-01	3.74E-02	1.01E-04	3.05E-03	9.03E-05	1.51E-05	4.56E-07	9.00E-06	4.70E-06	7.65E-06	0.90203	0.00010	0.06276	0.00013	0.05232	0.00013	0.05568	0.00078	0.72134	0.00013	0.71977	0.00014	0.71961	0.00017	0.71873	0.00017	335	1256
44.0	6.56E-01	5.57E-02	5.53E-04	4.68E-03	1.15E-04	3.10E-05	1.81E-05	2.65E-05	8.76E-06	2.66E-05	0.90270	0.00008	0.06225	0.00016	0.05153	0.00011	0.05689	0.00055	0.71986	0.00013	0.71843	0.00013	0.71833	0.00012	0.71749	0.00012	265	1033
2	6.85E-01	5.81E-02	1.23E-03	4.61E-03	2.23E-04	3.14E-05	2.08E-05	2.35E-05	1.71E-05	1.07E-05	0.90031	0.00005	0.06347	0.00008	0.05281	0.00010	0.05523	0.00090	0.72361	0.00039	0.71757	0.00008	0.71728	0.00011	0.71589	0.00011	467	2356
7	6.05E-01	5.17E-02	8.86E-04	4.04E-03	1.07E-04	3.39E-05	2.78E-05	2.85E-05	2.89E-05	2.27E-05	0.90044	0.00008	0.06326	0.00008	0.05288	0.00010	0.05298	0.00187	0.72437	0.00035	0.71946	0.00015	0.71915	0.00018	0.71734	0.00017	346	2851
12	6.93E-01	5.76E-02	4.76E-04	4.88E-03	1.38E-04	3.39E-05	2.08E-05	2.32E-05	2.13E-05	3.37E-05	0.90018	0.00005	0.06240	0.00013	0.05185	0.00008	0.05522	0.00066	0.72059	0.00025	0.71866	0.00010	0.71838	0.00013	0.71668	0.00012	375	2387
17	7.26E-01	6.13E-02	4.24E-04	5.05E-03	1.46E-04	2.85E-05	1.35E-05	5.62E-06	-1.63E-05	3.07E-05	0.90006	0.00007	0.06311	0.00007	0.05259	0.00011	0.05712	0.00042	0.72163	0.00020	0.71913	0.00009	0.71867	0.00010	0.71748	0.00010	78	2222
22	7.46E-01	6.34E-02	4.73E-04	5.34E-03	1.77E-04	3.29E-05	1.08E-05	1.35E-05	2.22E-06	2.27E-05	0.91993	0.00005	0.06227	0.00012	0.05181	0.00013	0.05526	0.00101	0.72058	0.00043	0.71881	0.00020	0.71878	0.00021	0.71732	0.00021	38	2180
28	7.11E-01	5.97E-02	4.84E-04	4.88E-03	1.46E-04	2.70E-05	1.91E-05	1.83E-05	3.02E-06	3.93E-05	0.90000	0.00004	0.06228	0.00005	0.05189	0.00009	0.05546	0.00038	0.72152	0.00026	0.71961	0.00008	0.71943	0.00013	0.71783	0.00013	251	2276
34	6.56E-01	5.53E-02	4.53E-04	4.53E-03	1.06E-04	2.84E-05	1.71E-05	2.34E-05	-2.71E-05	4.13E-05	0.90000	0.00007	0.06333	0.00011	0.05243	0.00011	0.05524	0.00079	0.72185	0.00017	0.71950	0.00008	0.71924	0.00009	0.71755	0.00008	215	2483
40	4.64E-01	3.93E-02	2.43E-04	3.27E-03	1.43E-04	2.87E-05	1.95E-05	1.34E-05	-1.30E-05	2.25E-05	0.90018	0.00008	0.06378	0.00017	0.05317	0.00019	0.05455	0.00098	0.72386	0.00056	0.72185	0.00022	0.72177	0.00027	0.71935	0.00027	167	3490

bold = above LoD, italic = below LoD

* after correction for REE^{2+} interference

[#] uncertainty c.+/-0.2mm unless underlined where uncertainty is +/- 2mm

LoD taken as typical daily 3SD of on-peak background

Appendix Table EA3 - LA-MC-ICP-MS data for calibration materials collected over various sessions

	Peak intensities*												$^{84}Sr/^{86}Sr$ ratios						$^{87}Sr/^{86}Sr$ ratios						Size of REE²⁺ & Ca_2 corr	SrCaPO17	CaPO17†	CaPO17
	Total	Total	Total	Total	Ca*	Dy* (81.5)	La* (81.5)	Yb* (86.5)	Yb* (85.5)	Er* (83.5)	mass bias	1se	mbc only	1se	REEcorr	1se	CaArcorr	1se	mbc only	1se	Rb corr only	1se	before CaPO corr	1se	(ppm)	(V)	(V)	(cps)
LoD (2SD)	[illegible]	[illegible]	[illegible]	[illegible]	[illegible]	[illegible]	[illegible]	[illegible]	[illegible]	[illegible]																		
modern shell																												
[illegible]	[illegible]	[illegible]	[illegible]	[illegible]	[illegible]	[illegible]	[illegible]	[illegible]	[illegible]	[illegible]	[illegible]	[illegible]	[illegible]	[illegible]	[illegible]	[illegible]	[illegible]	[illegible]	[illegible]	[illegible]	[illegible]	[illegible]	[illegible]	[illegible]	[illegible]	[illegible]	[illegible]	[illegible]
Durango apatite																												
[illegible]	[illegible]	[illegible]	[illegible]	[illegible]	[illegible]	[illegible]	[illegible]	[illegible]	[illegible]	[illegible]	[illegible]	[illegible]	[illegible]	[illegible]	[illegible]	[illegible]	[illegible]	[illegible]	[illegible]	[illegible]	[illegible]	[illegible]	[illegible]	[illegible]	[illegible]	[illegible]	[illegible]	[illegible]
[illegible]																												
[illegible]	[illegible]	[illegible]	[illegible]	[illegible]	[illegible]	[illegible]	[illegible]	[illegible]	[illegible]	[illegible]	[illegible]	[illegible]	[illegible]	[illegible]	[illegible]	[illegible]	[illegible]	[illegible]	[illegible]	[illegible]	[illegible]	[illegible]	[illegible]	[illegible]	[illegible]	[illegible]	[illegible]	[illegible]
[illegible]																												
[illegible]	[illegible]	[illegible]	[illegible]	[illegible]	[illegible]	[illegible]	[illegible]	[illegible]	[illegible]	[illegible]	[illegible]	[illegible]	[illegible]	[illegible]	[illegible]	[illegible]	[illegible]	[illegible]	[illegible]	[illegible]	[illegible]	[illegible]	[illegible]	[illegible]	[illegible]	[illegible]	[illegible]	[illegible]
[illegible]																												
[illegible]	[illegible]	[illegible]	[illegible]	[illegible]	[illegible]	[illegible]	[illegible]	[illegible]	[illegible]	[illegible]	[illegible]	[illegible]	[illegible]	[illegible]	[illegible]	[illegible]	[illegible]	[illegible]	[illegible]	[illegible]	[illegible]	[illegible]	[illegible]	[illegible]	[illegible]	[illegible]	[illegible]	[illegible]
[illegible]																												
[illegible]	[illegible]	[illegible]	[illegible]	[illegible]	[illegible]	[illegible]	[illegible]	[illegible]	[illegible]	[illegible]	[illegible]	[illegible]	[illegible]	[illegible]	[illegible]	[illegible]	[illegible]	[illegible]	[illegible]	[illegible]	[illegible]	[illegible]	[illegible]	[illegible]	[illegible]	[illegible]	[illegible]	[illegible]

Bold = above LoD; Italic = below LoD

* after correction for REE²⁺ interference

† calculated using TIMS $^{87}Sr/^{86}Sr$

LoD taken as typical daily 2SD of on-peak background